Dyes and Pigments 102 (2014) 301–307

Contents lists available at ScienceDirect

Dyes and Pigments

journal homepage: www.elsevier.com/locate/dyepig

A highly sensitive and selective ratiometric fluorescent sensor for Zn^{2+} ion based on ICT and FRET

Yang Ma [a,1], Haiyan Chen [b,1], Fang Wang [a], Srinivasulu Kambam [a], Yong Wang [a], Chun Mao [c,**], Xiaoqiang Chen [a,*]

[a] State Key Laboratory of Materials-Oriented Chemical Engineering, College of Chemistry and Chemical Engineering, Nanjing University of Technology, Nanjing 210009, China
[b] Department of Biomedical Engineering, School of Life Science and Technology, State Key Laboratory of Natural Medicines, China Pharmaceutical University, Nanjing 210009, China
[c] Jiangsu Key Laboratory of Biofunctional Materials, College of Chemistry and Materials Science, Nanjing Normal University, Nanjing 210023, China

ARTICLE INFO

Article history:
Received 20 May 2013
Received in revised form
7 November 2013
Accepted 10 November 2013
Available online 20 November 2013

Keywords:
Ratiometric sensor
Fluorescence
Zn^{2+}
Internal charge transfer
Fluorescence resonance energy transfer
Quinoline-based sensor

ABSTRACT

A ratiometric sensor (**QA**) for detecting Zn^{2+} with high sensitivity and selectivity was reported. The fluorescence changes of sensor upon the addition of Zn^{2+} were attributed to the conjugation of internal charge transfer and fluorescence resonance energy transfer mechanisms. There is a good linear relationship between the fluorescence ratio $I_{497\ nm}/I_{420\ nm}$ and the concentrations of Zn^{2+} ranging from 0 μM to 40 μM, which makes an effective ratiometric detection of Zn^{2+} ion. The limit of detection (LOD) was evaluated to be 33.6 nM. The imaging experiments indicated that **QA** is cell-permeable and can be used to detect Zn^{2+} within living cells with good selectivity over Cd^{2+}.

1. Introduction

Zinc is the second most abundant transition-metal ion and plays very important role in variety of physiological and pathological processes such as enzyme regulation, gene expression, catalytic function of protein, apoptosis and so on [1–7]. The disorder of zinc metabolism in biological systems may lead to a variety of diseases such as Alzheimer's disease, diabetes, epilepsy [8–14]. Therefore, developing effective methods for monitoring Zn^{2+} in living systems are very important for understanding the physiological and pathological role of zinc in nature. A variety of methods including electrochemical, photometric determination and electro-thermal atomic absorption spectrophotometry have been developed for analysis of zinc in environmental samples and for diagnosis of deficiencies in body tissue [15–17]. However, these methods have basic limitations in terms of equipment cost, complexity, sample processing and run times. Fluorogenic methods in conjunction with suitable probes are preferable approaches for the measurement of Zn^{2+} with high sensitivity, simplicity and real-time detection [18–21].

Although a number of fluorescent sensors based on various fluorophores including quinoline [22–31], fluorescein [32,33], coumarin [34,35], naphthalimide [36,37], BODIPY [38,39] and others [40,41] were developed for detection of zinc ions, it is still desirable to develop new Zn^{2+}-selective fluorescent sensors with extremely high affinity and good selectivity over other relevant metal ions. Since Frederickson et al. reported the first quinoline-based Zn^{2+} sensor [22], many fluorescent sensors based on 8-aminoquinoline structure have been developed for imaging Zn^{2+} in aqueous solution and in biological samples [26,29,42–50]. Because cadmium and zinc are in the same group of the periodic table and have similar properties, sensors based on aminoquinoline fluorophore usually suffered from the limitation in the effective distinguish between Zn^{2+} and Cd^{2+} [29,44,45,48]. Therefore, it is challenge to design a small molecular sensor based on aminoquinoline fluorophore which can selectively and sensitively detect Zn^{2+} in the presence of other cations, particularly Cd^{2+}.

Herein, based on internal charge transfer (ICT) and fluorescence resonance energy transfer (FRET) mechanisms, we report a new

* Corresponding author. Tel./fax: +86 025 83587856.
** Corresponding author. Tel.: +86 025 85891536.
E-mail addresses: maochun127@yahoo.com.cn (C. Mao), chenxq@njut.edu.cn (X. Chen).
[1] These authors contributed equally to this work.

0143-7208/$ – see front matter
http://dx.doi.org/10.1016/j.dyepig.2013.11.011

sensor (**QA**) bearing quinoline and anthracene fluorophores for the selective detection of Zn^{2+}. The fluorescent sensor based on ICT and FRET mechanisms has two advantages: one is the large shift between donor excitation and acceptor emission, which exclude any influence of excitation backscattering effects; the other is the presence of two well-separated emission bands with comparable intensities, which ensures accuracy in determining their intensities and ratios.

2. Experimental

2.1. Materials and equipments

Unless otherwise noted, materials were obtained from commercial suppliers and were used without further purification. Chromatography was carried out on silica gel 60 (230–400 mesh ASTM). ^1H and ^{13}C NMR spectra were recorded using Bruker 300/500. Mass spectra were obtained using a Waters Micromass Q-Tof mass spectrometer (Agilent 6530). Fluorescence emission spectra were obtained using RF-5301/PC spectrofluorophotometer. The imaging experiments were carried out using confocal laser scanning microscopy (Olympus FV-1000).

2.2. Synthesis

2.2.1. 2-Chloro-N-(quinolin-8-yl)acetamide (*1*)

Chloroacetyl chloride (0.15 mL) was dissolved in dry CH_2Cl_2 at 0 °C, and was added slowly to a stirred mixture of quinoline-8-amine (0.58 g, 4 mmol) and triethylamine (0.3 mL) in CH_2Cl_2 under N_2, the reaction mixture was stirred overnight at room temperature. The reaction mixture was quenched with distilled water and then was extracted with CH_2Cl_2. The combined organic layer was washed with 10% aqueous HCl solution and dried over anhydrous Na_2SO_4, and evaporated to afford solid product. The product was purified by recrystallization from ethanol to give analytically pure compound (0.82 g) in 93% yield. ^1H NMR ($CDCl_3$, 500 MHz) δ (ppm):10.90 (1H, s), 8.87–8.85 (1H, m), 8.77–8.74 (1H, m), 8.19–8.16 (1H, m), 7.58–7.53 (2H, m), 7.49–7.46 (1H, m), 4.31 (2H, s); ^{13}C NMR ($CDCl_3$, 75 MHz) δ (ppm):148.66, 136.27, 133.58, 127.95, 127.16, 122.52, 121.78, 116.64, 43.34.

2.2.2. 2-[(Pyridin-2-ylmethyl)-amino]-N-quinolin-8-yl-acetamide (*R-1*)

1 (0.88 g, 4 mmol) was dissolved in anhydrous CH_3CN and the solution was added dropwise to a stirred mixture of 2-aminomethylpyridine (0.86 g, 8 mmol), $NaHCO_3$ (0.69 g) and KI (0.66 g) at room temperature under N_2. The mixture was refluxed overnight. Then the resulting mixture was cooled to room temperature, filtered over gravity and the solvent was removed in vacuo. The residue was purified by column chromatography using CH_2Cl_2:CH_3OH (100:1) as the eluent to get pale orange solid (1.0 g) in 86% yield. ^1H NMR ($CDCl_3$, 300 MHz) δ (ppm): 11.43 (1H, s), 8.85–8.83 (2H, m), 8.60 (1H, d, J = 1.44 Hz), 8.19 (1H, d, J = 8.28 Hz), 7.70 (1H, t, J = 7.62 Hz), 7.56 (3H, d, J = 5.79 Hz), 7.48 (1H, q, J = 4.11 Hz), 7.27–7.19 (1H, m), 4.09 (2H, s), 3.63 (2H, s), 2.48 (1H, s); ^{13}C NMR ($CDCl_3$, 300 MHz) δ (ppm): 170.23, 158.90, 149.38, 148.40, 136.54, 136.20, 134.34, 128.09, 127.34, 122.65, 122.26, 121.72, 121.50, 116.65, 55.17, 53.31. TOF MS m/z = 293.1404 $[M + H^+]^+$, calc. for $C_{17}H_{17}N_4O$ = 293.1402.

2.2.3. 2-(Anthracen-9-ylmethyl-pridin-2-ylmethyl-amino)-N-quinolin-8-yl-acetamide (*QA*)

R-1 (0.58 g, 2 mmol) was dissolved in anhydrous CH_3CN and the solution was added dropwise to a stirred mixture of 9-(chloromethyl)anthracene (0.46 g, 2 mmol), $NaHCO_3$ (0.34 g) and KI (0.32 g) in anhydrous CH_3CN at room temperature under N_2. The mixture was refluxed overnight, then the resulting mixture was cooled to room temperature, filtered over gravity and the solvent was removed in vacuo. The residue was purified by column chromatography using CH_2Cl_2:CH_3OH (100:1) as the eluent to get yellow solid (0.66 g) in 69% yield. ^1H NMR ($CDCl_3$, 300 MHz) δ (ppm): 8.92 (1H, dd, J_1 = 4.17 Hz, J_2 = 1.65 Hz), 8.65 (1H, dd, J_1 = 5.73 Hz, J_2 = 3.30 Hz), 8.58 (1H, d, J = 4.26 Hz), 8.48 (2H, d, J = 8.76 Hz), 8.38 (1H, s), 8.15 (2H, m), 7.96–7.93 (2H, m), 7.73 (1H, td, J_1 = 7.65 Hz, J_2 = 1.74 Hz), 7.54 (1H, q, J = 4.20 Hz), 7.47–7.37 (6H, m), 7.25–7.24 (1H, m), 4.80 (2H, s), 4.19 (2H, s), 4.52 (2H, s); ^{13}C NMR ($CDCl_3$, 300 MHz) δ (ppm): 169.76, 158.13, 148.80, 138.77, 136.48, 134.33, 131.52, 131.37, 128.98, 128.32, 127.98, 127.31, 126.11, 124.82, 124.72, 124.54, 122.54, 121.49, 121.44, 116.42, 58.96, 53.39, 50.77. TOF MS m/z = 483.2181 $[M + H]^+$, calc. for $C_{32}H_{27}N_4O$ = 483.2185.

2.3. Cell culture and fluorescence imaging

MCF-7 cells were purchased from American Type Culture Collection (ATCC, USA), and were seeded in Laser scanning confocal microscope (LSCM) culture dishes with a density of 5×10^5 cells/well. The cell lines were cultured in RPMI-1640 medium supplemented with 10% (v/v) calf serum, penicillin (100 U mL^{-1}) and streptomycin (100 mg mL^{-1}). Cells were maintained at 37 °C in a humidified atmosphere containing 5% CO_2. When the whole cells took up 70%–80% space of culture dishes, the cells were first incubated with 10 μM **QA** in culture media for 1 h at 37 °C. Then the cells were further treated with 100 μM Zn^{2+} or Cd^{2+} in culture media containing 2% DMSO for 15 min at 37 °C. After washing with phosphate buffered saline (PBS) to remove the remaining Zn^{2+} or Cd^{2+}, the cells were imaged by confocal laser scanning microscopy (Olympus FV-1000). Zn^{2+} imaging experiment after removal the intracellular Zn^{2+} was carried out by incubation with TPEN for 15 min. The band paths for green channel and blue channel are 500–600 nm and 425–475 nm respectively. The excitation wavelength is 488 nm for green channel and 405 nm for blue channel.

2.4. Detection limit

Fluorescence titration was carried out in HEPES-buffered solution (10 mM HEPES, 50% (v/v) DMSO, pH = 7.4) to calculate the detection limit, the detection limit is then calculated with the equation:

$$\text{detection limit} = 3\sigma_{bi}/m$$

where σ_{bi} is the standard deviation of blank measurements, m is the slope between intensity versus sample concentration.

2.5. The calculation of K_d

The fluorescent intensity data were fit to the following equation to calculate K_d [51]:

$$F = \left(\alpha_1 K_d + \alpha_2 \left[Zn^{2+}\right]\right)[\mathbf{QA}]_{total} / \left(\left[Zn^{2+}\right] + K_d\right).$$

where F is the fluorescence intensity, α_1, α_2 represent a proportionality parameter of fluorescent species, $[\mathbf{QA}]_{total}$ means the total concentration of the **QA**. Finally, Origin 8.0 software was used to fit above nonlinear plot to give the K_d value.

3. Results and discussion

3.1. Synthesis of compound *QA*

The synthetic route of compound **QA** was shown in Scheme 1. Firstly, **R-1** was synthesized. Then, the reaction of **R-1** and 9-(chloromethyl)anthracene in the presence of $NaHCO_3$ and KI in CH_3CN afford the final product **QA** with the yield of 69%. The synthesized compound **QA** was fully characterized by ^1H, ^{13}C NMR and Q-Tof mass spectrometer (see Supplementary Data). These characterizations confirmed the formation of compound **QA**.

3.2. Fluorescence studies with various metal ions

After obtained the sensor, the selectivities of **QA** to various metal ions were first examined in DMSO-HEPES buffer (pH = 7.4, 10 mM, 1:1 v/v). The fluorescence spectra were obtained by excitation at 330 nm, and various metal ions including Hg^{2+}, Na^+, Mg^{2+}, Cs^{2+}, Cr^{3+}, Ni^{2+},Ca^{2+}, Zn^{2+}, Cd^{2+}, Pb^{2+}, Ag^+, Fe^{3+}, Fe^{2+}, Li^+, Al^{3+}, Mn^{2+} and Cu^{2+} were used to evaluate the selectivity of **QA**. As shown in Fig. 1, when no metal ions were added, **QA** showed the structured emission band at 400 nm, 420 nm and 445 nm typical of the anthracene moiety. Upon the addition of 10 equiv. of various metal ions, Zn^{2+} caused dramatic fluorescent enhancement at 497 nm along with a decrease of emission intensity of the structured emission band. In contrast, other metal ions such as Na^+, Mg^{2+}, Cs^{2+}, Cr^{3+}, Ni^{2+}, Ca^{2+}, Cd^{2+}, Pb^{2+}, Ag^+, Fe^{3+}, Fe^{2+}, Li^+, Al^{3+}, Mn^{2+} produced the negligible changes at 497 nm while Cu^{2+} and Hg^{2+} led to the entire quenching of fluorescence. It is noteworthy that the addition of Cd^{2+} did not induce the increase of fluorescent intensity at 497 nm, even though cadmium and zinc are in the same group of the periodic table and have similar properties. Indeed, compared with the quinoline-based sensors reported previously [24,44,48–50,52–54], the present sensor provided better selectivity towards Zn^{2+} over Cd^{2+}. It is proposed that the introduction of anthracene fluorophore disable the binding between Cd^{2+} with aminoquinoline moiety. Further, a competition experiment was also performed by adding Zn^{2+} (10 equiv) to the sensor in the presence of other metal ions (10 equiv.), which showed that no obvious interference was observed in its fluorescence except for Cu^{2+} and Hg^{2+}, which caused the emission ratio of 497 nm–420 nm quenched (Fig. 2).

The concentration-dependent fluorescence spectra were further examined in DMSO-HEPES buffer (pH = 7.4, 1:1 v/v). As shown in the Fig. 3a, in the absence of Zn^{2+}, the emission spectrum of **QA** exhibits a structured emission band with maxima at 400 nm, 420 nm and 445 nm typical of the anthracene moiety. Upon addition of increasing Zn^{2+}, the structured emission band of the anthracene unit gradually decreases along with a new red-shift emission band at 497 nm and a well-defined isoemission point at 460 nm. An obvious increase in fluorescence intensity ratio ($I_{497\ nm}/I_{420\ nm}$) changed from 0.6 to 7.5

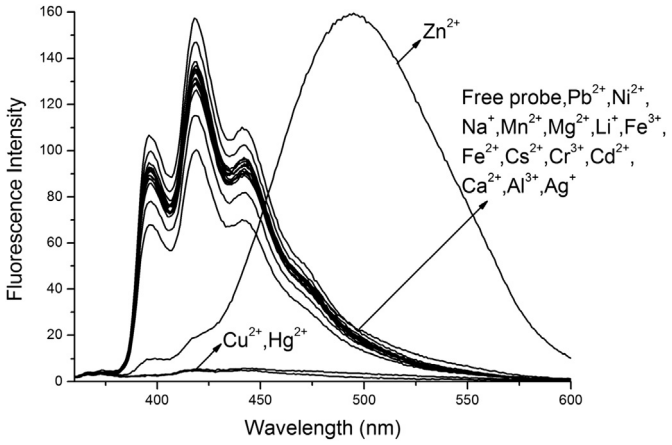

Fig. 1. Fluorescence responses (λ_{ex} = 330 nm) of 10 μM probe **QA** towards various metal ions in DMSO-HEPES buffer (pH = 7.4, 10 mM, 1:1 v/v).

(Fig. 3b) is also observed. The intensity ratios at 497 and 420 nm ($I_{497\ nm}/I_{420\ nm}$) increase until the addition of 8 equiv. Zn^{2+}. Besides, a good linearity between the fluorescence intensity ratios and the concentrations of Zn^{2+} is obtained in the range of 0 μM–40 μM (Fig. S1). According to fluorescence titration data under the concentration of

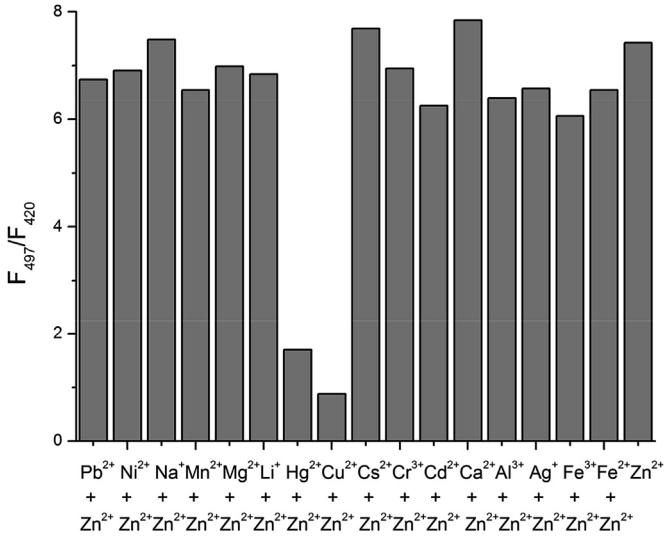

Fig. 2. The ratio fluorescence responses ($I_{497\ nm}/I_{420\ nm}$) of **QA** (10 μM) containing 100 μM Zn^{2+} to the selected metal ions: 10 equiv of Pb^{2+}, Ni^{2+}, Na^+, Mn^{2+}, Mg^{2+}, Li^+, Hg^{2+}, Cu^{2+}, Cs^{2+}, Cr^{3+}, Ca^{2+}, Al^{3+}, Ag^+, Fe^{3+}, Fe^{2+} in DMSO-HEPES buffer (pH = 7.4, 10 mM, 1:1 v/v).

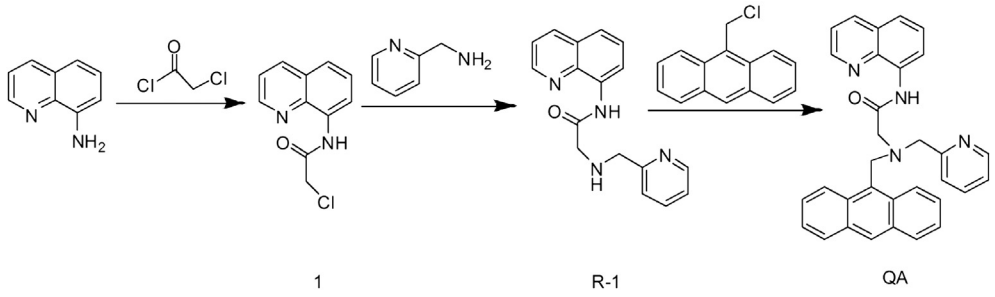

Scheme 1. The synthesis of **QA**.

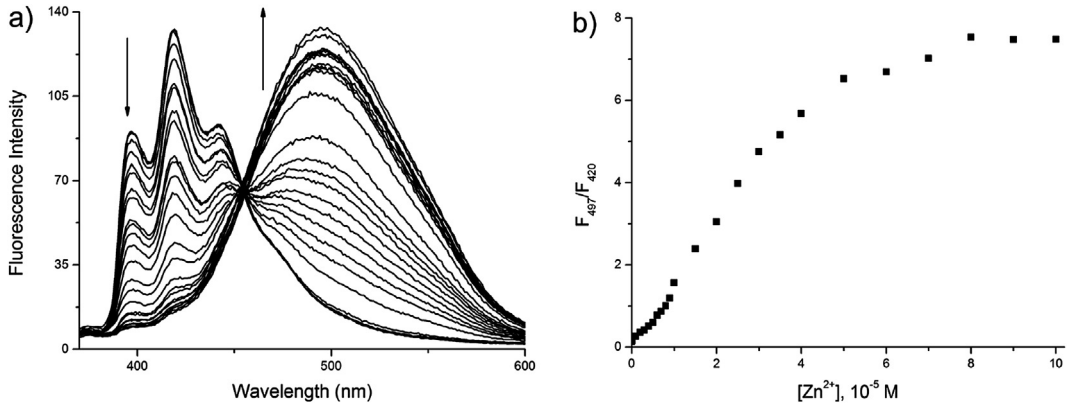

Fig. 3. a) Fluorescence titration of **QA** (10 μM) in DMSO-HEPES buffer (pH = 7.4, 10 mM, 1:1 v/v); b) The plot of fluorescence ratios ($I_{497\ nm}/I_{420\ nm}$) versus the concentration of Zn^{2+}.

Zn^{2+} in the range from 0 to 40 μM, the limit of detection (LOD) was calculated to be 33.6 nM.

3.3. The binding between sensor *QA* and Zn^{2+}

A Job's plot analysis was carried out for quantifying the stoichiometry of the complex of **QA** and Zn^{2+}. As shown in Fig. 4,

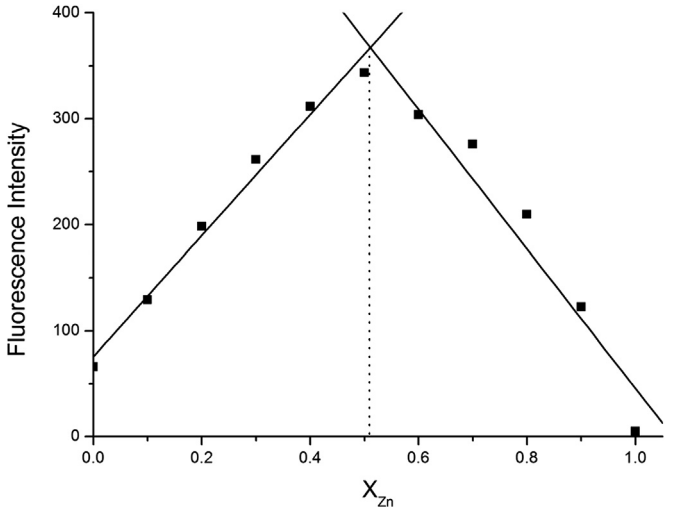

Fig. 4. Job's plot for determining the stoichiometry of probe **QA** and Zn^{2+} in the HEPES-buffered solution (10 mM HEPES, 50% (v/v) DMSO, pH = 7.4). The total concentration of probe and Zn^{2+} is 100 μM, $X_{Zn} = [Zn^{2+}]/([Zn^{2+}] + [\mathbf{QA}])$, monitored at 497 nm.

when the fluorescent intensity ratio $I_{497\ nm}/I_{420\ nm}$ was plotted against molar factions of **QA** and Zn^{2+} under the constant total concentration (100 μM), the maximum point was observed at a mole fraction of 0.5, which means **QA** binds Zn^{2+} with a 1:1 stoichiometry. The binding between **QA** and Zn^{2+} was identified further by the high-resolution ESI-MS spectrum. In Fig. 5, the *m/z* peak at 545.1345 appeared, which corresponds to the molecular ion peak of $[\mathbf{QA}\text{-}H^{+}+Zn^{2+}]^{+}$. The **QA** and Zn^{2+} binding affinity was evaluated by fluorescence titration experiment (Fig. S2), and the dissociation constant (K_d) for Zn^{2+} binding to **QA** is calculated to be 52 ± 8 μM, which is relatively high compared to previously reported Zn ion sensor with the dissociation constant at pM level [34]. The reason should be attributed to that the binding affinity of the sensor with mono pyridine moiety is much weaker than that with double pyridine moieties. The low-affinity Zn^{2+} sensor is potential in monitoring the Zn^{2+} concentration in synaptic vesicles of many excitatory forebrain neurons where the concentration of Zn^{2+} was reported to be in the micro- to millimolar range [55,56].

On the mechanism of fluorescence changes induced by Zn^{2+}, we proposed that the complexation between Zn^{2+} and *N* atoms in **QA** provided the "off–on" response for quinoline fluorophore *via* internal charge transfer effect, which is similar to the previous sensors containing 8-aminoquinoline moiety [26,31,44]. Owing to the emission band of anthracene fluorophore overlaps the excitation band of quinoline fluorophore (Fig. S3), then FRET effect from donor (anthracene) to acceptor (quinoline) occurred, leading to the decrease of the emission intensity at 420 nm accompanied by the increase of the emission intensity at 497 nm (Fig. 6).

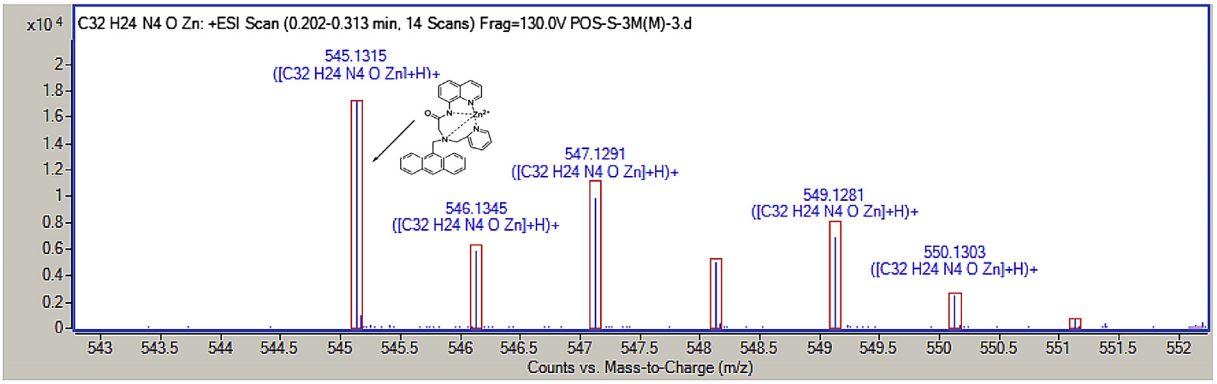

Fig. 5. TOF-mass of the complex of **QA** with Zn^{2+}.

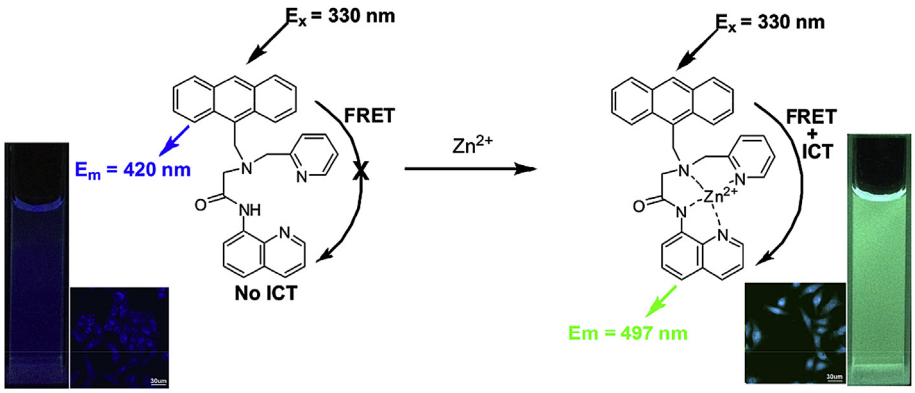

Fig. 6. The mechanism for detecting Zn^{2+}.

3.4. *The bio-imaging of sensor **QA** in living cells*

The ability of **QA** to image zinc ions in living cells was also evaluated (Fig. 7). After MCF-7 cells incubated with 10 μM **QA** for 1 h at 37 °C, a blue fluorescence was observed by confocal laser scanning microscopy (Fig. 7b) while green channel showed negligible fluorescence (Fig. 7c). However, when 100 μM of Zn^{2+} was added and incubated for 15 min, the intense green fluorescence appeared from the green channel (Fig. 7g) and the overlay picture of blue and green channels exhibited the fluorescence of cells changed into bluish green from blue (Fig. S4). Addition of the cell-permeable chelator TPEN (N,N,N′,N′-tetrakis(−)[2-pyridylmethyl]-ethylenediamine) recovered the blue fluorescence and faded the green fluorescence, which confirms that the fluorescence changes result from Zn(II) coordination (Fig. 7j and k). The further imaging with the treatment of Cd^{2+} indicated that **QA** can be used to image Zn^{2+} without the interference of Cd^{2+} within living cells (Fig. S4).

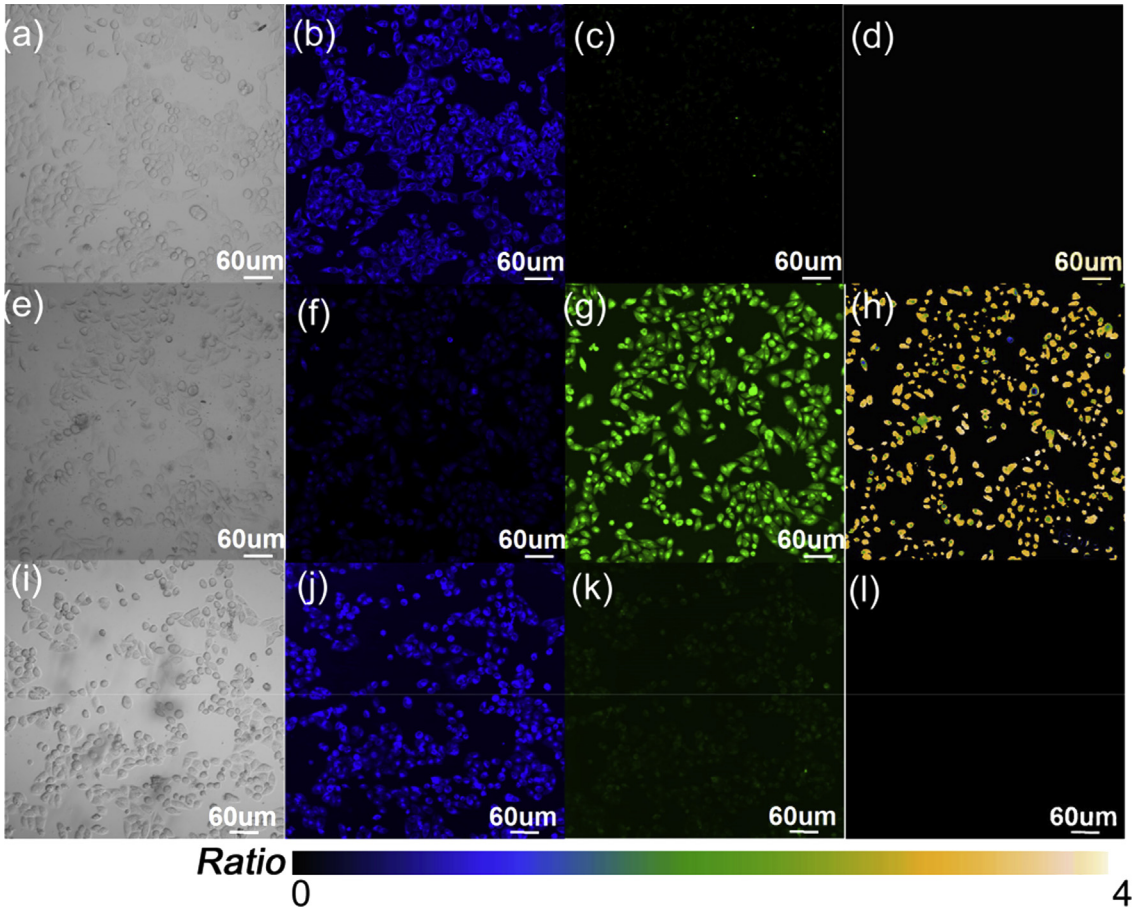

Fig. 7. Confocal fluorescence images of intracellular Zn^{2+} in MCF-7 cells. MCF-7 cells incubated with probe **QA** (10 μM) (in 2% DMSO v:v) at 37 °C for 1 h (top); **QA** stained cells were exposed to 100 μM Zn^{2+} at 37 °C for 15 min (middle); and sequestration of intracellular Zn^{2+} by addition of 200 μM TPEN for 15 min (bottom). (a), (e), (i) Bright-field images. (b), (f), (j) Fluorescence images with emission collected at 425–475 nm. (c), (g), (k) Fluorescence images with emission collected at 500–600 nm. (d), (h), (l) Ratio images $F_{500-600}$ nm/$F_{425-475}$ nm. The blue channel images were collected upon excitation at 405 nm and the green ones were collected upon excitation at 488 nm. Scale bar: 60 μm, ratio bar: 0–4.

4. Conclusions

In conclusion, we reported a new ratiometric fluorescence sensor (**QA**) bearing quinoline and anthracene fluorophores. The sensor shows a selective fluorescence changes with Zn^{2+} over other metal ions. Free sensor appears a strong fluorescence at 400 nm, 420 nm and 445 nm, corresponding to the emission band of anthracene fluorophore. Upon the binding of Zn^{2+} ion, the emission band of anthracene fluorophore is gradually quenched while a new emission peak at around 497 nm appears. The fluorescence changes of sensor upon the addition of Zn^{2+} were attributed to the composite of internal charge transfer and fluorescence resonance energy transfer mechanisms. In addition, there is a good linear relationship between the fluorescence ratio $I_{497\ nm}/I_{420\ nm}$ and the concentration of Zn^{2+} ranging from 0 μM to 40 μM, which makes an effective ratiometric detection of Zn^{2+} ion. The imaging experiments demonstrated **QA** are potential to trace zinc ions in living cells.

Acknowledgments

This work was supported by grants from NSF of China (21002049, 81371684 and 21376117), the Natural Science Foundation of the Jiangsu Higher Education Institutions of China (Grant No. 10KJB150005), and the Scientific Research Foundation for the Returned Overseas Chinese Scholars of State Education Ministry.

Appendix A. Supplementary data

Supplementary data related to this article can be found at http://dx.doi.org/10.1016/j.dyepig.2013.11.011.

References

[1] O'Halloran TV. Transition metals in control of gene expression. Science 1993;261:715–25.
[2] Falchuk KH. The molecular basis for the role of zinc in developmental biology. Mol Cell Biochem 1998;188:41–8.
[3] Jiang PJ, Guo ZJ. Fluorescent detection of zinc in biological systems: recent development on the design of chemosensors and biosensors. Coord Chem Rev 2004;248:205–29.
[4] Maret W. Zinc biochemistry, physiology, and homeostasis – recent insights and current trends. Biometals 2001;14:187–90.
[5] Burdette SC, Lippard SJ. Meeting of the minds: metalloneurochemistry. Proc Natl Acad Sci U S A 2003;100:3605–10.
[6] Berg JM, Shi Y. The galvanization of biology: a growing appreciation for the roles of zinc. Science 1996;271:1081–5.
[7] Vallee BL, Falchuk KH. The biochemical basis of zinc physiology. Physiol Rev 1993;73:79–118.
[8] Bush AI. The metallobiology of Alzheimer's disease. Trends Neurosci 2003;26:207–14.
[9] Frederickson CJ, Koh JY, Bush AI. The neurobiology of zinc in health and disease. Nat Rev Neurosci 2005;6:449–62.
[10] Chausmer AB. Zinc, insulin and diabetes. J Am Coll Nutr 1998;17:109–15.
[11] Smith JL, Xiong S, Markesbery WR, Lovell MA. Altered expression of zinc transporters-4 and -6 in mild cognitive impairment, early and late Alzheimer's disease brain. Neuroscience 2006;140:879–88.
[12] Ho E. Zinc deficiency, DNA damage and cancer risk. Nutr Biochem 2004;15:572–8.
[13] Sladek R. A genome-wide association study identifies novel risk loci for type 2 diabetes. Nature 2007;445:881–5.
[14] Lu M, Fu D. Structure of the zinc transporter YiiP. Science 2007;317:1746–8.
[15] Ge B, Scheller FW, Lisdat F. Electrochemistry of immobilized CuZnSOD and FeSOD and their interaction with superoxide radicals. Biosens Bioelectron 2003;18:295–302.
[16] Urbanova N, Kadar M, Toth K, Bogati B, Andruch V, Bitter I. Fluorescent iminodiacetamide derivatives as potential ionophores for optical zinc ion-selective sensors. Anal Sci 2008;24:727–33.
[17] Tewari PK, Singh AK. Thiosalicylic acid-immobilized amberlite XAD-2: metal sorption behaviour and applications in estimation of metal ions by flame atomic absorption spectrometry. Analyst 2000;125:2350–5.
[18] Chen XQ, Zhou GD, Peng XJ, Yoon J. Biosensors and chemosensors based on the optical responses of polydiacetylenes. Chem Soc Rev 2012;41:4610–30.
[19] Chen XQ, Pradhan T, Wang F, Kim JS, Yoon J. Fluorescent chemosensors based on spiroring-opening of xanthenes and related derivatives. Chem Rev 2012;112:1910–56.
[20] Guo ZQ, Song NR, Moon JH, Kim M, Jun EJ, Choi J, et al. A benzobisimidazolium-based fluorescent and colorimetric chemosensor for CO_2. J Am Chem Soc 2012;134:17846–9.
[21] Song NR, Moon JH, Jun EJ, Choi J, Kim SJ, Lee JY, et al. Cyclic benzobisimidazolium derivative for the selective fluorescent recognition of HSO_4^- via a combination of C–H hydrogen bonds and charge interactions. Chem Sci 2013;4:1765–71.
[22] Frederickson CJ, Kasarskis EJ, Ringo D, Frederickson RE. A quinoline fluorescence method for visualizing and assaying the histochemically reactive zinc(bouton zinc) in the brain. J Neurosci Methods 1987;20:91–103.
[23] Fahrni CJ, O'Halloran TV. Aqueous coordination chemistry of quinoline-based fluorescence probes for the biological chemistry of zinc. J Am Chem Soc 1999;121:11448–58.
[24] Hanaoka K, Kikuchi K, Kojima H, Urano Y, Nagano T. Development of a zinc ion-selective luminescent lanthanide chemosensor for biological applications. J Am Chem Soc 2004;126:12470–6.
[25] Wang HH, Gan Q, Wang XJ, Xue L, Liu SH, Jiang H. A water-soluble, small molecular fluorescent sensor with femtomolar sensitivity for zinc ion. Org Lett 2007;9:4995–8.
[26] Zhang Y, Guo XF, Si WX, Jia LH, Qian XH. Ratiometric and water-soluble fluorescent zinc sensor of carboxamidoquinoline with an alkoxyethylamino chain as receptor. Org Lett 2008;10:473–6.
[27] Xue L, Liu Q, Jiang H. Ratiometric Zn^{2+} fluorescent sensor and new approach for sensing Cd^{2+} by ratiometric displacement. Org Lett 2009;11:3454–7.
[28] Ravikumar I, Ghosh P. Zinc(II) and PPi selective fluorescence OFF-ON-OFF functionality of a chemosensor in physiological conditions. Inorg Chem 2011;50:4229–31.
[29] Chen XY, Shi J, Li YM, Wang FL, Wu X, Guo QX, et al. Two-photon fluorescent probes of biological Zn(II) derived from 7-hydroxyquinoline. Org Lett 2009;11:4426–9.
[30] Xue L, Liu C, Jiang H. Highly sensitive and selective fluorescent sensor for distinguishing cadmium from zinc ions in aqueous media. Org Lett 2009;11:1655–8.
[31] Zhou XY, Yu BR, Guo YL, Tang XL, Zhang HH, Liu WS. Both visual and fluorescent sensor for Zn^{2+} based on quinoline platform. Inorg Chem 2010;49:4002–7.
[32] Hirano T, Kikuchi K, Urano Y, Nagano T. Improvement and biological applications of fluorescent probes for zinc, ZnAFs. J Am Chem Soc 2002;124:6555–62.
[33] Walkup GK, Burdette SC, Lippard SJ, Tsien RY. A new cell-permeable fluorescent probe for Zn^{2+}. J Am Chem Soc 2000;122:5644–5.
[34] Komatsu K, Urano Y, Kojima H, Nagano T. Development of an iminocoumarin-based zinc sensor suitable for ratiometric fluorescence imaging of neuronal zinc. J Am Chem Soc 2007;129:13447–54.
[35] Xu ZC, Liu X, Pan J, Spring DR. Coumarin-derived transformable fluorescent sensor for Zn^{2+}. Chem Commun 2012;48:4764–6.
[36] Xu ZC, Baek KH, Kim HN, Cui JN, Qian XH, Spring DR, et al. Zn^{2+}-triggered amide tautomerization produces a highly Zn^{2+}-selective, cell-permeable, and ratiometric fluorescent sensor. J Am Chem Soc 2010;132:601–10.
[37] Lu X, Zhu W, Xie Y, Li X, Gao Y, Li F, et al. Near-infrared core-substituted naphthalenediimide fluorescent chemosensors for zinc ions: ligand effect on PET and ICT channels. Chem Eur J 2010;16:8355–64.
[38] Wu Y, Peng X, Guo B, Fan J, Zhang Z, Wang J. Boron dipyrromethene fluorophore based fluorescence sensor for the selective imaging of Zn(II) in living cells. Org Biomol Chem 2005;3:1387–92.
[39] Cao J, Zhao C, Wang X, Zhang Y, Zhu W. Target-triggered deprotonation of 6-hydroxyindole-based BODIPY: specially switch on NIR fluorescence upon selectively binding to Zn^{2+}. Chem Commun 2012;48:9897–9.
[40] Guo Z, Kim GH, Shin I, Yoon J. A cyanine-based fluorescent sensor for detecting endogenous zinc ions in live cells and organisms. Biomaterials 2012;33:7818–27.
[41] Wang F, Moon JH, Nandhakumar R, Kang B, Kim D, Kim KM, et al. Zn^{2+}-induced conformational changes in a binaphthyl-pyrene derivative monitored by using fluorescence and CD spectroscopy. Chem Commun 2013;49:7228–30.
[42] Rastogi SK, Pal P, Aston DE, Bitterwolf TE, Branen AL. 8-Aminoquinoline functionalized silica nanoparticles: a fluorescent nanosensor for detection of divalent zinc in aqueous and in yeast cell suspension. ACS Appl Mater Interfaces 2011;3:1731–9.
[43] Sutariya PG, Modi NR, Pandya A, Joshi BK, Joshi KV, Shobhana K, et al. An ICT based "turn on/off" quinoline armed calix[4]arene fluoroionophore: its sensing efficiency towards fluoride from waste water and Zn^{2+} from blood serum. Analyst 2012;137:5491–4.
[44] Du JJ, Fan JL, Peng XJ, Li HL, Sun SG. The quinoline derivative of ratiometric and sensitive fluorescent zinc probe based on deprotonation. Sens Actuators B 2010;144:337–41.
[45] Gao CJ, Jin XJ, Yan XH, An P, Zhang Y, Liu LL, et al. A small molecular fluorescent sensor for highly selectivity of zinc ion. Sens Actuators B 2013;176:775–81.
[46] Cai YL, Meng XM, Wang SX, Zhu MZ, Pan ZW, Guo QX. A quinoline based fluorescent probe that can distinguish zinc(II) from cadmium(II) in water. Tetrahedron Lett 2013;54:1125–8.

[47] Lee HG, Lee JH, Jang SP, Hwang IH, Kim SJ, Kim Y, et al. Zinc selective chemosensors based on the flexible dipicolylamine and quinoline. Inorg Chim Acta 2013;394:542–51.
[48] Zhou XB, Lu YG, Zhu JF, Chan WH, Lee AM, Chan PS, et al. Ratiometric fluorescent Zn^{2+} chemosensor constructed by appending a pair of carboxamidoquinoline on 1,2-diaminocyclohexane scaffold. Tetrahedron 2011;67:3412–9.
[49] Zhang LW, Duan DZ, Cui XM, Sun JY, Fang JG. A selective and sensitive fluorescence probe for imaging endogenous zinc in living cells. Tetrahedron 2013;69:15–21.
[50] Ma Y, Wang F, Kambam S, Chen X. A quinoline-based fluorescent chemosensor for distinguishing cadmium from zinc ions using cysteine as an auxiliary reagent. Sens Actuators B 2013;188:1116–22.
[51] Du PW, Lippard SJ. A highly selective turn-on colorimetric, red fluorescent sensor for detecting mobile zinc in living cells. Inorg Chem 2010;49:10753–5.
[52] Mikata Y, Ugai A, Yasuda K, Itami S, Tamotsu S, Konno H, et al. Quinoline-based, glucose-pendant fluorescent zinc probes. Chem Biol 2012;9:2064–75.
[53] Meng XM, Wang SX, Li YM, Zhu MZ, Guo QX. 6-Substituted quinoline-based ratiometric two-photon fluorescent probes for biological Zn^{2+} detection. Chem Commun 2012;48:4196–8.
[54] Kim JH, Hwang IH, Jang SP, Kang J, Kim S, Noh I, et al. Zinc sensors with lower binding affinities for cellular imaging. Dalton Trans 2013;42:5500–7.
[55] Frederickson CJ, Klitenick MA, Manton WI, Kirkpatrick JB. Cytoarchitectonic distribution of zinc in the hippocampus of man and the rat. Brain Res 1983;273:335–9.
[56] Komatsu K, Kikuchi K, Kojima H, Urano Y, Nagano T. Selective zinc sensor molecules with various affinities for Zn^{2+}, revealing dynamics and regional distribution of synaptically released Zn^{2+} in hippocampal slices. J Am Chem Soc 2005;127:10197–204.